Materials Letters 290 (2021) 129453

Contents lists available at ScienceDirect

Materials Letters

journal homepage: www.elsevier.com/locate/mlblue

Observation of hydrogen diffusion channel and hydrogen trap in 304 austenitic stainless steel

Hui-yun Zhang [a,b], Yan-mei Li [d], Wei Liang [a,c,*], Liu-wei Zheng [a,c,*]

[a] College of Materials Science and Engineering, Taiyuan University of Technology, Taiyuan 030024, PR China
[b] Department of Mechanical Manufacturing Engineering, Shanxi Engineering Vocational College, Taiyuan 030009, Shanxi Province, PR China
[c] Instrumental Analysis Center, Taiyuan University of Technology, Taiyuan 030600, PR China
[d] The State Key Laboratory of Rolling and Automation Northeastern University, Shenyang 110819, China

ARTICLE INFO

Article history:
Received 22 January 2021
Received in revised form 28 January 2021
Accepted 29 January 2021
Available online 10 February 2021

Keywords:
Austenite stainless steel
Grain boundary
α′-Martensite
Hydrogen diffusion channel
Hydrogen trap

ABSTRACT

Hydrogen embrittlement (HE) involves hydrogen-defect interactions at multiple-length scales. However, the challenge of measuring the precise location of hydrogen atoms limits our understanding. We used time of flight-secondary ion mass spectrometer (TOF-SIMS) to observe hydrogen localization in 304 austenitic stainless steel. A large amount of hydrogen observed at grain boundary in cold-rolled steel contains strain-induced α′-martensite provides direct evidence that α′-martensite act as hydrogen diffusion channel and grain boundaries act as trapping sites, which achieves a mechanistic understanding of hydrogen materials interactions and facilitates the development of hydrogen-resistant steels.

1. Introduction

Although the phenomenon was first identified a century ago, hydrogen embrittlement (HE) remains an extremely important unsolved industrial challenge [1]. Let's start with a series of accident cases [2]: During World War II, a British fighter plane crashed due to a broken main shaft of its engine; in 1975, a stainless steel pipe burst suddenly in an American refinery, causing explosion and fire; the connecting bolts of supercharger oil inlet pipe and supercharger of a gasoline engine in China have been broken for many times. After long-term observation and research, scientists have found out that HE may be the culprit of these malignant accidents. Atomic hydrogen enters into the material, moves and accumulates. When the local hydrogen concentration reaches the critical value, the material will fracture [3].

To understand both hydrogen diffusion channel and hydrogen trap, we require information about the position of hydrogen atoms at the nanometer length scale [1]. However, the combination of the low level of interaction between an electron and hydrogen and the extremely fast diffusion of hydrogen in steels renders it extremely difficult to experimentally determine the location of hydrogen by electron microscopy. Mass spectroscopy technique was suited to identifying the location of hydrogen because it can be identified by its ratio of mass to charge state. In the present study, the localization of hydrogen in 304 austenitic stainless steel was detected by Time of flight-Secondary Ion Mass Spectrometer (TOF-SIMS), which provided a direct basis for the analysis of the hydrogen diffusion channel and hydrogen trap.

2. Material and methods

A 5 mm-thick solution-treated 304 austenitic stainless steel with the composition of Fe–18.26Cr–1.11Mn–0.41Si–8Ni–0.04C–0.04N–0.029P–0.001S (wt %) was used for the present study. The as-received steels were cold-rolled to 2 mm and 2.5 mm, respectively. All the plates were reheated at 1050 ℃ for 20 min, followed by water quenching. Then the 2.5 mm plate was cold-rolled to 2 mm. In this way, the plates were cold-rolled to 2 mm-thick with different thickness reductions of 0% (as-solution) and 20%, excluding the effect of thickness on HE.

The longitudinal section of electropolished specimens were characterized using an Oxford electron back-scattered diffraction (EBSD). The specimens were electrochemically charged with hydrogen in a 1 mol/L NaOH aqueous solution containing 1 g/L NH_4SCN with a current density of 50 mA/cm^2 for 48 h at room

* Corresponding authors at: College of Materials Science and Engineering, Taiyuan University of Technology, Taiyuan 030024, PR China.
E-mail addresses: liangwei@tyut.edu.cn (W. Liang), zhengliuwei@tyut.edu.cn (L.-w. Zheng).

https://doi.org/10.1016/j.matlet.2021.129453
0167-577X/

temperature. Their tensile properties were tested on a material testing machine (DNS 200) with a strain rate 3.3×10^{-4} /s. The fracture morphology of tensile specimens was characterized by a high resolution scanning electron microscope (HSSEM, Tescan Mira 3). The hydrogen distribution of the samples was detected via TOF-SIMS equipped on a Gallium FIB-SEM system (S8000G) at electron beam of 1nA and voltage of 30kv.

The solution-treated sample was marked as S, the cold-rolled sample was named as CR and the corresponding hydrogen-charged sample was added with -H. For example, CR-H refers to the cold-rolled sample after hydrogen charging.

3. Results and discussion

Fig. 1a and d show the inverse pole figure (IPF) maps. Fig. 1b and e refer phase images (yellow for martensite phase and blue for austenite phase) of specimens. It is obvious that the S microstructure is composed of single austenite phase and annealing twins, while the CR microstructure consists of deformed austenite phase, twins and martensite phase. Compared with the almost negligible martensite in S, CR contains 18.1% martensite phase formed near the junctions of grain boundary and twin boundary (appearing blue in Fig. 1f).

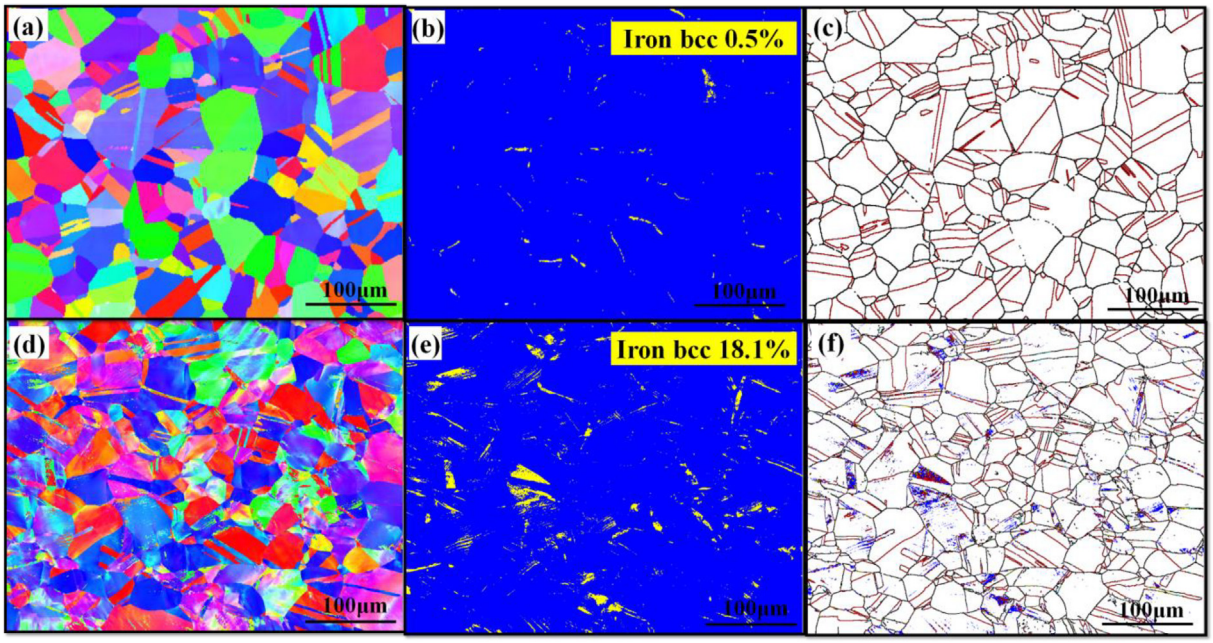

Fig. 1. IPF maps (a) S (d) CR; Phase images (b) S (e) CR; Twin boundaries (c) S (f) CR.

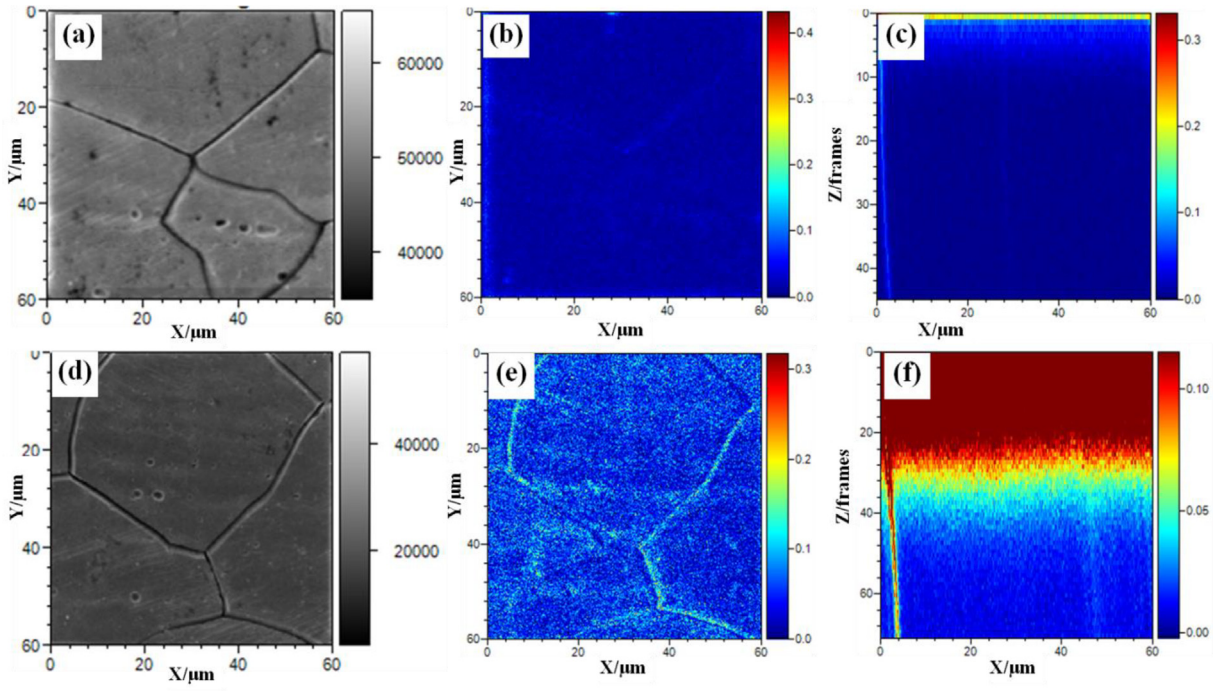

Fig. 2. Hydrogen localization of samples after hydrogen charging. (a)-(c) S-H; (d)-(f) CR-H.

The stacking fault energy (SFE) of metastable austenitic stainless steel is low, and lower SFE leads to increase the mobility of extended dislocations, favors the formation of planar deformation structure which enables the generation of energetically favorable nucleation sites for martensitic transformation [4].

Fig. 2 shows the localization of hydrogen in S-H and CR-H samples detected by TOF-SIMS. Fig. 2a and d are the SEM images of two samples; Fig. 2b and e refer to hydrogen localization of the sample surface corresponding to the SEM image area in the X-Y direction; Fig. 2c and f show hydrogen localization of the same area in the X-Z direction. The penetration depth of hydrogen in CR-H is much greater than that in S-H sample. From Fig. 2b, less hydrogen can be seen at the grain boundary in S-H, which demonstrates that the grain boundary of experimental steel is hydrogen trap. From Fig. 2e, we can see a large amount of hydrogen obviously segregated around grain boundaries in CR-H, which demonstrates that α′-martensite formed by cold-rolling is hydrogen diffusion channel, providing a way to accelerate the hydrogen transportation to the matrix during electrochemical hydrogen charging, then hydrogen is captured by the grain boundary. When the amount of strain-induced α′-martensite reaches a certain value, strain-induced α′-martensite connects with each other and experiences the variation of morphology from point to sheet seen from Fig. 1f. It implies an effective diffusion path in austenite is created [5].

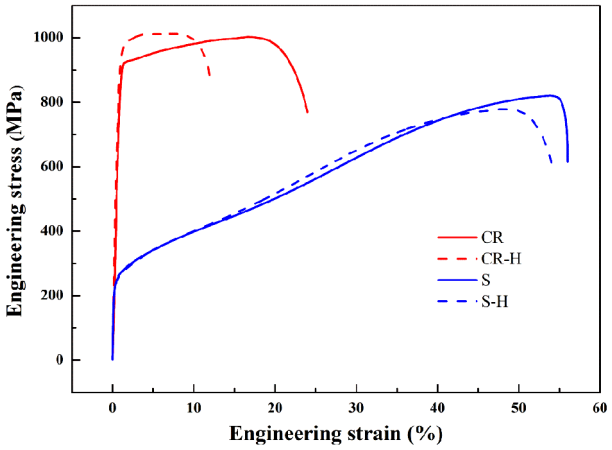

Fig. 3. Stress–strain curves of experimental steels before and after hydrogen charging.

Fig. 3 shows the tensile properties of the specimens. Whether hydrogen charged or not, the yield strength (Rp0.2) and tensile strength of CR increased obviously at the cost of the elongation in comparison to S, which due to the increase of dislocation density and α′-martensite content introduced by deformation. Samples exhibited insignificant changes in strength after hydrogen charged, while the reduction of plasticity had different performance. The elongation of S after hydrogen charged decreased from 54% to 50%, and the reduction rate was only 7.4%, while the elongation of CR was reduced from 24% to 12%, with the reduction rate was 50%.

Fig. 4 illustrates the fracture morphologies for the specimens after hydrogen charging. It can be seen that the fracture of all experimental steels show two regions with different characteristics: ductile fracture occurred in the central region of samples and brittle fracture occurred near the fracture edge. The thickness of the S-H brittle layer was 29.81 μm, whereas that of CR-H was 245.23 μm. At the same time, it can be seen from Fig. 4b and d that the brittle fracture mode changes from cleavage fracture to intergranular fracture after cold rolling.

The sharp decrease in plasticity may be associated with the "wetting" effect. The α′-martensite formed by cold-rolling fully or partially surrounded the grains of matrix phase, forming so-called "wetting" effect in the solid state [6]. In turn, Fig. 2e shows

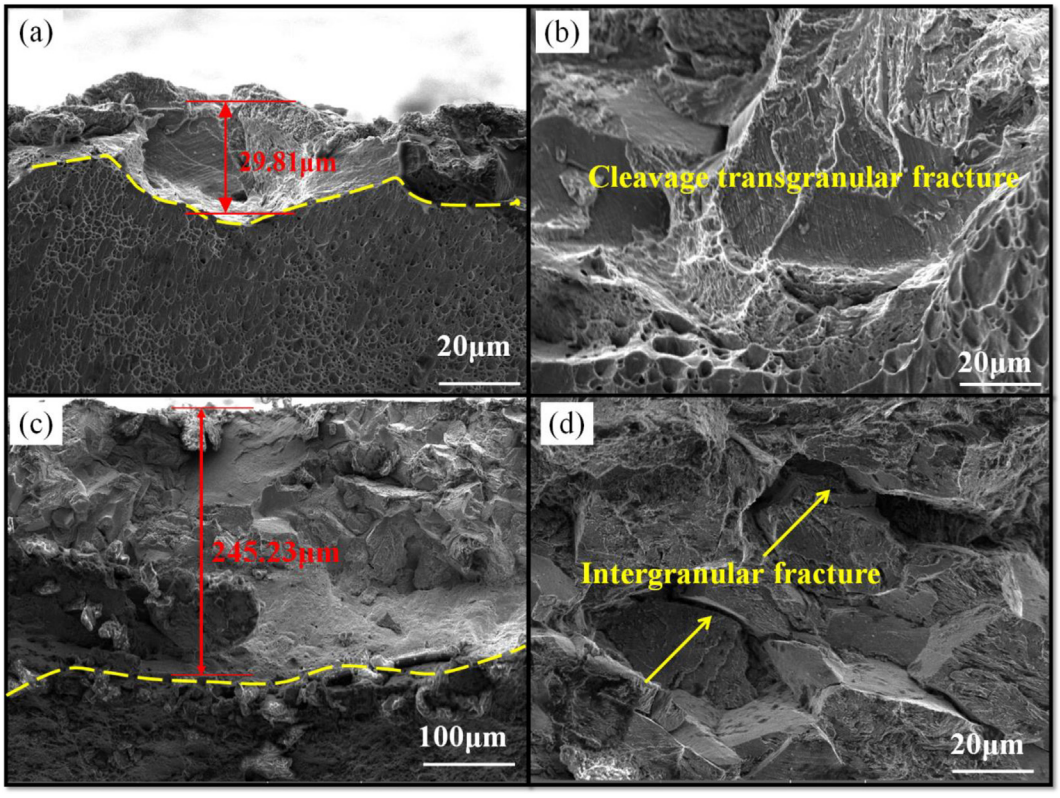

Fig. 4. The fracture of experimental steels after hydrogen charging. (a) (b) S-H; (c) (d) CR-H.

that a segregation of hydrogen along grain boundaries, thereby corroborating the possible occurrence of "wetting" of grain boundaries by the martensite phase. The grain boundaries wetted with the (hard and brittle) martensite phase, decreased the overall ductility of the material [7] and because it is harder, microcracks tend to initiate through this phase [8]. After hydrogen charging, hydrogen trapped by grain boundaries weakened the interatomic bonds, further reduced plasticity and led cracks propagate through the grain boundaries under tensile, i.e. intergranular fracture.

It can be concluded from the above experimental results, compared with the solution-treated sample, during the process of electrochemical hydrogen charging, hydrogen rapidly diffused to α′-martensite formed by cold-rolling due to the high hydrogen diffusivity and the low hydrogen diffusivity in the matrix (austenite) [9]. Then the grain boundaries wetted by martensite phase trapped the hydrogen in α′-martensite quickly, which reduced the HE resistance and led to intergranular fracture. In summary, hydrogen induced intergranular fracture which observed in the cold-rolled specimen result from the interaction among α′-martensite, grain boundaries and hydrogen [10].

4. Conclusion

The interaction of grain boundary and martensite with hydrogen is acquired by comparing the HE phenomenon in solution-treated and cold-rolled type 304 austenitic stainless steel. As a comparison, no martensite is formed and the negligible hydrogen is only found at the grain boundary of the solution-treated sample, and the cleavage fracture occurs after tensile. After cold-rolling, the obvious segregation of hydrogen can be seen at the grain boundary, because martensite is formed near the junctions of grain boundary and twin boundary, a large amount of hydrogen diffuses through the martensite which as a diffusion channel and is captured by the grain boundary which as a hydrogen trap, consistent with that intergranular fracture occurs after tensile.

CRediT authorship contribution statement

Hui-yun Zhang: Writing - original draft, Conceptualization, Methodology. **Yan-mei Li:** Visualization, Investigation. **Wei Liang:** Writing - review & editing. **Liu-wei Zheng:** Software, Resources.

Declaration of Competing Interest

The authors declare that they have no known competing financial interests or personal relationships that could have appeared to influence the work reported in this paper.

Acknowledgement

This work is supported by the Shanxi International Cooperation Project (approval number: 201603D421026) and Shanxi Engineering Vocational College Key Projects (KYF-201903).

References

[1] Y.-S. Chen, L.u. Hongzhou, J. Liang, Science 367 (2020) 171–175.
[2] K.H. Lo, C.H. Shek, J.K.L. Lai, Mater. Sci. Eng.: R: Rep. 65 (4–6) (2009) 39–104.
[3] M. Dadfarnia, A. Nagao, S. Wang, M.L. Martin, B.P. Somerday, P. Sofronis, Int. J. Fract. 196 (1–2) (2015) 223–243.
[4] G. Sun, L. Du, J. Hu, B. Zhang, R.D.K. Misra, Mater. Sci. Eng., A 746 (2019) 341–355.
[5] W. Qu, C. Gu, J. Zheng, Y. Zhao, Z. Hua, Int. J. Hydrogen Energy 44 (17) (2019) 8751–8758.
[6] A.S. Gornakova, B.B. Straumal, A.N. Nekrasov, A. Kilmametov, N.S. Afonikova, J. Mater. Eng. Perform. 27 (10) (2018) 4989–4992.
[7] A.B. Straumal, K.V. Tsoy, I.A. Mazilkin, A.N. Nekrasov, K. Bryła, Arch. Metall. Mater. 64 (2019) 869–873.
[8] S.V. Zherebtsov, E.A. Kudryavtsev, G.A. Salishchev, B.B. Straumal, S.L. Semiatin, Acta Mater. 121 (2016) 152–163.
[9] X. Chen, C. Zhou, J. Zheng, L. Zhang, Int. J. Hydrogen Energy 43 (6) (2018) 3342–3352.
[10] A. Oudriss, J. Creus, J. Bouhattate, E. Conforto, C. Berziou, C. Savall, X. Feaugas, Acta Mater. 60 (19) (2012) 6814–6828.